A Simple Index for Predicting the Susceptibility to Solidification Cracking

The crack susceptibility of an Al alloy can be reduced if the filler metal reduces the maximum steepness of its curve of temperature T vs. square root of fraction solid $(f_S)^{1/2}$

BY S. KOU

ABSTRACT

The present study proposed to use the maximum $|dT/d(f_S)^{1/2}|$ of an alloy as a simple index for its susceptibility to solidification cracking. The index was based on a recent criterion for cracking that considered the phase diagram, solidification shrinkage, strain rate, cooling rate, and liquid feeding. However, other factors may also affect the susceptibility, e.g., the dihedral angle and secondary phases. Curves of T vs. $(f_S)^{1/2}$ of Al alloys were plotted to find the maximum $|dT/d(f_S)^{1/2}|$ using commercial thermodynamic software package Pandat and database PanAluminum based on the Scheil solidification model of no solid-state diffusion. Several critical predictions were made based on the index, including the crack susceptibility reduction by Al filler metals, the relative crack susceptibility of wrought Al alloys 2014, 2024, 2219, 6061, and 7075, and the most crack susceptible compositions of binary Al-Si, Al-Cu, and Al-Mg alloys. These predictions were verified by reported crack susceptibility tests and published filler metal guides. Although the predicted crack susceptibility of Al-Mg alloys was too high, it was not caused by the index but by the Scheil model because it doesn't consider diffusion. It was explained that, because of the very high (17.5 wt-%) Mg solubility in solid Al, significant Mg diffusion from the interdendritic liquid into Al-rich dendrites can occur and reduce the maximum $|dT/d(f_S)^{1/2}|$ significantly, consistent with the good weldability of Al-Mg alloys.

KEYWORDS

• Solidification Cracking • Aluminum Alloys • Filler Metals
• Crack Susceptibility Index • Fraction Solid • 2014 Al • 2024 Al • 2219 Al
• 7075 Al • 6061 Al • 4043 Al Filler Metal • 4145 Al Filler Metal
• Al-Si Alloys • Al-Cu Alloys • Al-Mg Alloys

Introduction

Many alloys are susceptible to cracking during solidification, which is called solidification cracking in welding (Ref. 1) and hot tearing in casting (Refs. 2–4). Figure 1 shows an example of solidification cracking. A 1.6-mm-thick 6061 Al sheet was bead-on-plate welded by using the gas tungsten arc welding (GTAW) process without a filler metal.

The mushy zone (a semisolid) between the weld pool and the completely solidified weld metal is weak and susceptible to cracking. As the weld pool moves forward, both the solidified weld metal and the portion of the workpiece behind the pool cool and contract. The higher density of the solid than the liquid causes the weld metal to contract during solidification. Solidification shrinkage can be as much as 6.6% in the case of Al (Ref. 2). The thermal expansion coefficient causes both the solidified weld metal and the workpiece to contract during cooling. Thus, both solidification shrinkage and thermal contraction induce tensile strain in the mushy zone. The more tightly the workpiece is clamped down or connected to a rigid body, the more tensile strain is induced by its thermal contraction.

The semisolid material in the mushy zone has little strength because it consists of dendritic grains that are still separated by liquid. The problem is that the semisolid also has little ductility during the terminal stage of solidification when there is insufficient liquid between grains for them to move and rearrange themselves to accommodate tensile strains without cracking.

Numerous theories or models have been proposed for hot tearing (Ref. 5). Some of them assumed the mushy zone will crack when the tensile stress, strain, or strain rate exceeds a critical value. Apblett and Pellini's strain theory in 1954 (Ref. 6) assumed that grains are separated by thin liquid films near the end of solidification and that cracking occurs when the highly localized strains in the liquid films finally exceed the critical limit they can withstand. Prokhorov's theory in 1962 (Ref. 7) focused mainly on the thermomechanical factor of cracking, assuming that cracking can occur if the rate of strain accumulation with temperature drop $d\varepsilon/dT$ exceeds a critical value. The model of Feurer in 1977 (Ref. 8), on the other hand, focused mainly

S. KOU (kou@engr.wisc.edu) *is professor in the Department of Materials Science and Engineering, University of Wisconsin, Madison, Wis.*

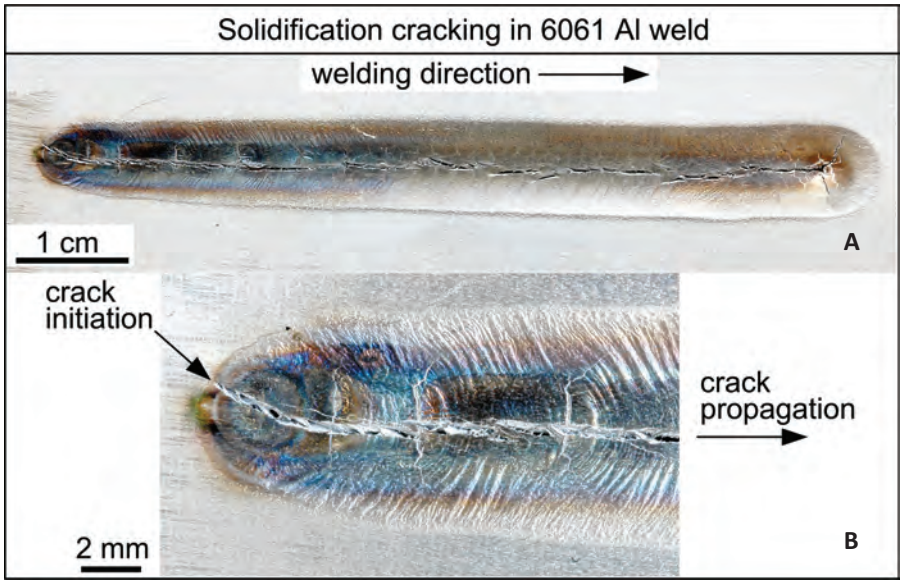

Fig. 1 — Solidification cracking in 6061 Al alloy. A — Overview; B — close-up view. Crack initiates at starting end of weld, from a nucleation site that is either inside the weld or at its surface. Gas tungsten arc welding, 90 A, 10 V and 2.5 mm/s, bead-on-plate welding, no filler metal, full penetration through 1.6-mm-thick sheet.

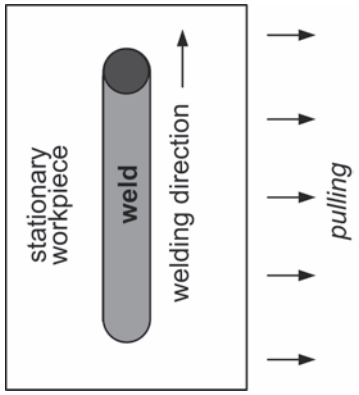

Fig. 2 — Testing susceptibility to solidification cracking by applying tensile deformation normal to the welding direction. Coniglio et al. (Refs. 12, 13) and Matsuda et al. (Ref. 15).

on liquid feeding of the shrinking mushy zone. It assumed cracking can occur if volumetric shrinkage exceeds volumetric feeding.

The model of Clyne and Davies in 1981 (Ref. 9) assumed: 1) stress relief through mass and liquid feeding in $0.40 < f_S < 0.90$, 2) grain separation in $0.90 < f_S < 0.99$, and 3) grain bridging in $0.99 < f_S < 1.0$, where f_S is fraction solid. The ratio t_V/t_R was taken as the susceptibility to hot tearing, where t_V is the vulnerable time period in $0.90 < f_S < 0.99$ and t_R is the time available for stress relief in $0.40 < f_S < 0.90$. These times were calculated assuming different cooling conditions in casting.

The prominent RDG model of Rappaz, Drezet, and Gremaud (Ref. 10), proposed in 1999 for hot tearing, considered both tensile deformation and solidification shrinkage. A steady-state, mass-balance differential equation involving both solid and liquid was integrated to determine the velocity distribution of the interdendritic liquid in the mushy zone. The velocity was then related to Darcy's law (for flow through a porous structure) and further integrated to find the pressure drop across the mushy zone Δp_{max}. It was assumed that, when the interdendritic liquid pressure falls below a certain cavitation pressure, a void may form and give rise to a crack at the root of the dendrites. The cavitation depression, an unknown key value of the model, was set to 2 kPa (0.02 atm).

The RDG model was applied to solidification cracking in welding by Drezet et al. (Ref. 11). The grain coalescence temperature was assumed to be the temperature at fraction solid $f_S = 0.98$ or the eutectic temperature if fraction eutectic $f_E > 0.02$. A hot cracking susceptibility (HCS) was calculated for an Al-Cu-Li alloy, and filler metal 4047 Al was shown to reduce the HCS. No comparison with experimental data was shown.

The RDG model (Ref. 10) was also applied by Coniglio et al. (Refs. 12, 13) to solidification cracking in Al welds, who indicated that cavitation in the mushy zone due to pressure drop is not likely to occur in view of the very high pressure (10^3 to 10^4 atm) required for vapor pore nucleation (Ref. 3). Instead, they proposed a porosity-based crack initiation model. Pores were suggested to form from preexisting pore nuclei instead of by cavitation caused by pressure drops. A crack growth model was also proposed to relate the crack growth rate to the local strain rate through mass balance.

It became clear more recently that the strain rate, instead of the strain itself, can play a critical role in solidification cracking. The existence of a critical strain rate above which solidification cracking occurs was confirmed experimentally by Matsuda et al. (Ref. 14) and more recently by Coniglio et al. (Refs. 12, 13). The latter used the test method illustrated in Fig. 2, with an extensometer (not shown) positioned at the bottom surface of the workpiece across the width of the weld. A similar method was used by Matsuda et al. (Ref. 15), but without an extensometer. The advantage of using the extensometer is that the local strain rate in the weld can be determined, instead of the global strain rate in the workpiece. The former, not the latter, is responsible for solidification cracking.

Lippold (Ref. 16) recently reviewed five theories or models that were developed or used to study solidification cracking in welding, including the shrinkage-brittleness theory of some early investigators including Pumphrey and Jennings (Ref. 17), the strain theory of Apblett and Pellini (Ref. 6), the generalized theory of Borland (Ref. 18), the modified generalized theory of Matsuda and coworkers (Ref. 19), and the technological strength theory of Prokhorov (Ref. 7). It was pointed out that the shrinkage-

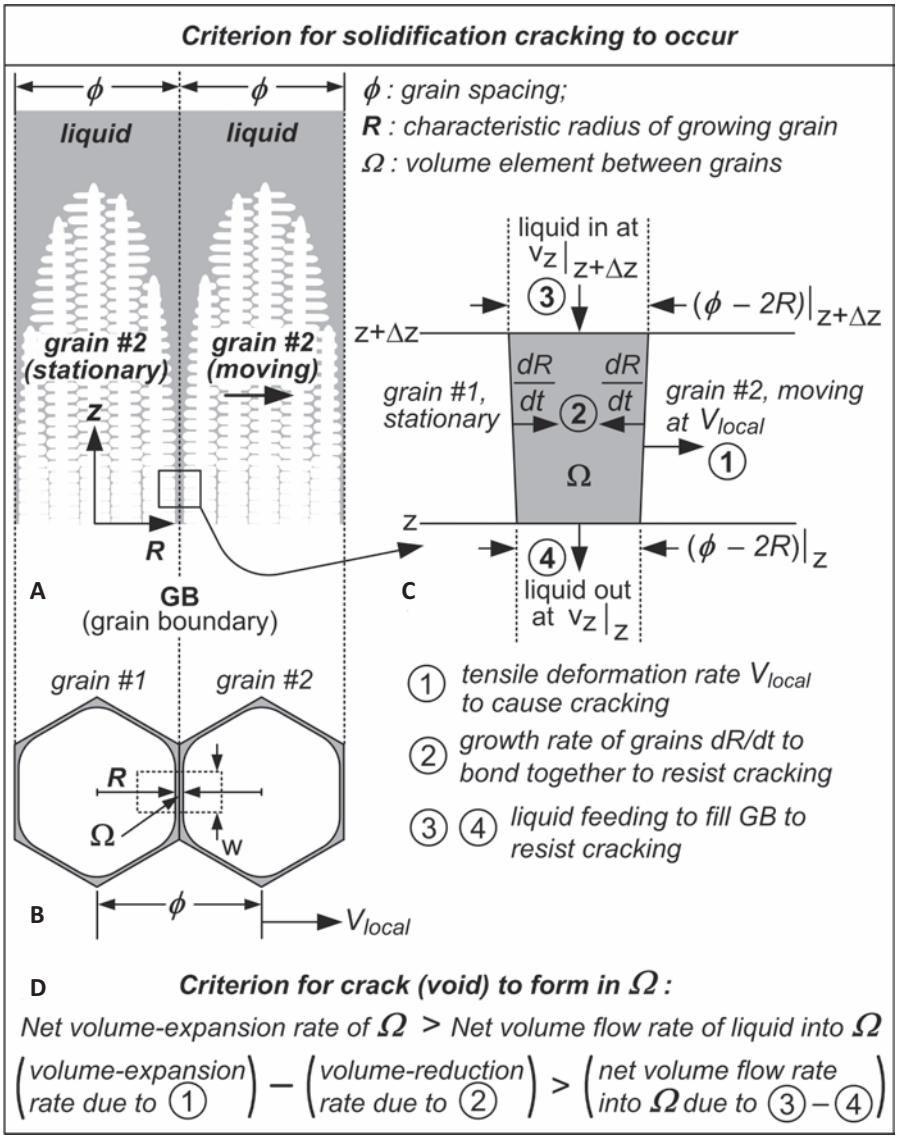

Fig. 3 — Criterion for cracking during solidification in casting and welding. A — Longitudinal cross section of growing grains; B — transverse cross section near end of solidification; C — boxed area in A enlarged to show volume element Ω; D — criterion for cracking. Modified from Kou (Ref. 20).

brittleness theory suggested that grains begin to interact with each other and form a rigid network at the so-called "coherency temperature" and that cracking can only occur after some solid-solid bridging has occurred, which allows strain to accumulate in the structure. It was also pointed out that there is usually no evidence of solid-solid fracture on the surface of a solidification crack to support theories that suggest cracking by breaking solid-solid bridges between growing grains, such as the shrinkage-brittleness theory (Ref. 17) and the generalized theory of Borland (Ref. 18). It was commented that the strain theory of Pellini (Ref. 6) is consistent with the typically smooth dendritic fracture surfaces of the weld metal. It was also commented that Prokhorov's theory (Ref. 7) is useful for explaining the ductility/strain contribution, though it does not address the metallurgical or fracture aspects of solidification cracking.

A Criterion for Cracking During Solidification

Based on solidification concepts and transport phenomena, a criterion for cracking to occur during solidification in casting and welding was proposed by Kou (Ref. 20). The criterion led to an index for predicting the crack susceptibility. Unlike previous investigators, Kou (Ref. 20) considered the grain boundary, which is critical because cracking occurs along the grain boundary. Considering two columnar dendritic grains growing side by side, he related cracking along the grain boundary to: 1) separation of grains from each other under lateral tensile deformation to cause cracking, 2) lateral growth of grains toward each other to bond together to resist cracking, and 3) liquid feeding along the grain boundary to resist cracking.

Figure 3A shows schematically the longitudinal cross section of two columnar dendritic grains growing side by side in the axial direction *z*. The grain spacing is ϕ. The characteristic radius of the growing grains is *R*, which is a function of *z*, that is, *R(z)*. These grains can be similar to those at the centerline of the mushy zone, where cracking occurs most often during welding. The two grains are being separated by local tensile deformation at V_{local} in the lateral direction. The tensile deformation can be self-induced by solidification shrinkage and thermal contraction or caused by an external force if it is applied (Fig. 2). For the purpose of discussion, grain No. 1 is assumed stationary and grain No. 2 moving to the right at the speed of V_{local}.

Figure 3B shows schematically the transverse cross section of two columnar dendritic grains. A control volume Ω of width *w* can be set up at the grain boundary to analyze the susceptibility to solidification cracking. As illustrated in Fig. 3C, it is the volume of the space, not the liquid, between the grains that is responsible for cracking to occur. V_{local} is the local deformation rate to separate the grains and cause cracking. It increases the space in Ω. *dR/dt* is the rate the grains grow toward each other to bond together to resist cracking. It decreases the space in Ω. v_z is the velocity of the liquid in the *z*-direction to feed the grain boundary and resist cracking.

The space in Ω increases as the grain on the right moves away at the local speed of V_{local} and decreases as the two grains grow toward each other

at the rate of $2R/dt$, where t is time. The net increase of space in Ω is the former minus the latter. The intergranular liquid flows at the velocity v_z in the negative z-direction to feed the grain boundary. The net inward flow is the inward flow at $z + Dz$ minus the outward flow at z. Since Ω is very narrow, the liquid between the grains is in the form of a thin film during terminal solidification. As illustrated in Fig. 3D, when V_{local} exceeds the ability of the liquid film in Ω to accommodate it, a tear or crack (that is a void) can be initiated. Thus, provided preexisting nucleation sites are available, a crack can form in Ω if the rate of net space increase in Ω exceeds the rate of net volumetric flow into Ω, that is, if

$$\begin{aligned} & w\left[V_{local}\Delta z\right]-w\left[\frac{d(2R)}{dt}\Delta z\right] \\ & > w\left[\left((\phi-2R)v_z\right)_{z+\Delta z}\right] \\ & -w\left[\left((\phi-2R)v_z\right)_z\right] \end{aligned} \quad (1)$$

Upon dividing by wDz and taking the limit of Dz → zero, Equation 1 becomes

$$V_{local} > \frac{d(2R)}{dt}+\frac{d}{dz}\left[(\phi-2R)v_z\right] \quad (2)$$

Figure 4 shows how the growth rate of grains dR/dt can be related to the square root of the fraction solid $(f_S)^{1/2}$. The transverse cross-sectional area of the growing grain a increases from zero at the beginning of solidification to A at the end. It is round initially and hexagonal at the end. The characteristic grain radius R is a function of the axial distance z, that is, $R(z)$. Toward the end of solidification, the liquid within the grains is negligible in quantity as compared to the solid (Ref. 20), and thus $f_S = a/A$. Since the transverse cross-section of the grain is essentially round, as shown by the broken circle of the same area, R is proportional to $(a/A)^{1/2}$. In fact, when $(a/A)^{1/2}$ is plotted against $R/(\phi/2)$, a nearly perfect straight line is obtained (Ref. 20), that is, the characteristic grain radius can be related to the fraction solid f_S as follows:

$$\frac{R}{\phi/2}=\left(\frac{a}{A}\right)^{1/2}=\left(f_S\right)^{1/2} \quad (3)$$

The solidification shrinkage b can be considered by modifying the characteristic grain radius R as $R(1 - b)^{1/2}$ (Ref. 20). Considering b, Equation 3 and $d(f_S)^{1/2}/dt = [d(f_S)^{1/2}/dT](dT/dt)$ (where T is temperature and t time), Equation 2 can be rewritten as follows:

$$\left\{\begin{aligned} & V_{local} > \phi\sqrt{1-\beta}\,\frac{d\sqrt{f_S}}{dT}\frac{dT}{dt} \\ & +\phi\frac{d}{dz}\left[\left(1-\sqrt{1-\beta}\sqrt{f_S}\right)v_z\right] \end{aligned}\right\}_{\sqrt{f_S}\to 1} \quad (4)$$

$$\left\{\begin{aligned} & \frac{d\varepsilon_{local}}{dt} > \sqrt{1-\beta}\,\frac{d\sqrt{f_S}}{dT}\frac{dT}{dt} \\ & +\frac{d}{dz}\left[\left(1-\sqrt{1-\beta}\sqrt{f_S}\right)v_z\right] \end{aligned}\right\}_{\sqrt{f_S}\to 1} \quad (5)$$

$$\left\{\begin{aligned} & \frac{d\varepsilon_{local}}{dT} > \sqrt{1-\beta}\,\frac{d\sqrt{f_S}}{dT} \\ & \text{(separation)}\quad\text{(growth)} \\ & +\frac{1}{(dT/dt)}\frac{d}{dz}\left[\left(1-\sqrt{1-\beta}\sqrt{f_S}\right)v_z\right] \\ & \text{(feeding)} \end{aligned}\right\}_{\sqrt{f_S}\to 1} \quad (6)$$

Equation 5 is derived from Equation 4 by dividing it with ϕ and letting $V_{local} = dD_{local}/dt$, where D_{local} is the local deformation and the local strain $\varepsilon_{local} = D_{local}/\phi$. When further divided by the cooling rate dT/dt, Equation 5 becomes Equation 6.

The separation term on the LHS (left hand side) of Equations 4, 5, or 6 is associated with the tensile deformation to separate two neighboring grains. On the RHS (right hand side), the growth term is associated with the growth of the two grains toward each other, and the feeding term the liquid feeding to fill the grain boundary.

The criterion (Ref. 20) shows that cracking is more likely under 1) faster tensile deformation rate V_{local} or strain rate $d\varepsilon/dt$, 2) slower cooling rate dT/dt, and 3) faster rate of strain accumulation with temperature drop $d\varepsilon_{local}/dT$. The last one is consistent with Prokhorov's model (Ref. 7). However, Prokhorov's model considers the "brittleness temperature range," which is not necessarily the range near $(f_S)^{1/2} = 1$.

The criterion represents the necessary condition for cracking to occur during solidification, not the sufficient condition. To be sufficient, preexisting nucleation sites for cracks must be available (Ref. 21). This will be further discussed subsequently.

An Index for Crack Susceptibility

Based on the criterion, an index can be proposed for the susceptibility of an alloy to cracking during solidification, that is, $|dT/d(f_S^{1/2})|$ near $(f_S)^{1/2} = 1$. First, as already shown in Fig. 4, the growth rate for the grains to bond together to resist cracking decreases with increasing $|dT/d(f_S^{1/2})|$ near $(f_S)^{1/2} = 1$. Second, as illustrated in Fig. 5, liquid feeding to fill the grain boundary and resist cracking also decreases with increasing $|dT/d(f_S^{1/2})|$ near $(f_S)^{1/2} = 1$. A large $|dz/dR|$ means the grain radius R hardly increases as the axial distance z decreases, that is, a long liquid channel between the two neighboring grains. As mentioned previously, near $(f_S)^{1/2} = 1$ the grain radius R is proportional to $(f_S)^{1/2}$. Thus, $|dz/dR|$ is proportional to $|dz/d(f_S^{1/2})|$, which equals $|dT/d(f_S^{1/2})|/|dT/dz|$. Therefore, under the same axial temperature gradient dT/dz, a larger $|dT/d(f_S^{1/2})|$ near $(f_S)^{1/2} = 1$ means a larger $|dz/dR|$ near $(f_S)^{1/2} = 1$, and hence, a longer liquid channel — Fig. 5B. According to the Hagen-Poiseuille law (Ref. 22), the volumetric flow rate of a liquid through a channel decreases with increasing channel length (and decreasing channel opening), due to the resistance to flow caused by the viscosity of the liquid.

Thus, increasing $|dT/d(f_S^{1/2})|$ near $(f_S)^{1/2} = 1$ increases the crack susceptibility by decreasing the growth rate dR/dt that is needed for the grains to bond together to resist cracking. It also increases the length of the liquid channel along the grain boundary. A longer grain boundary channel hinders the liquid feeding that is needed to fill the grain boundary to resist cracking. In fact, from a mechanics point of view, a longer grain boundary channel is also easier to open up and propagate under tension. Thus, $|dT/d(f_S^{1/2})|$ near $(f_S)^{1/2} = 1$ can be

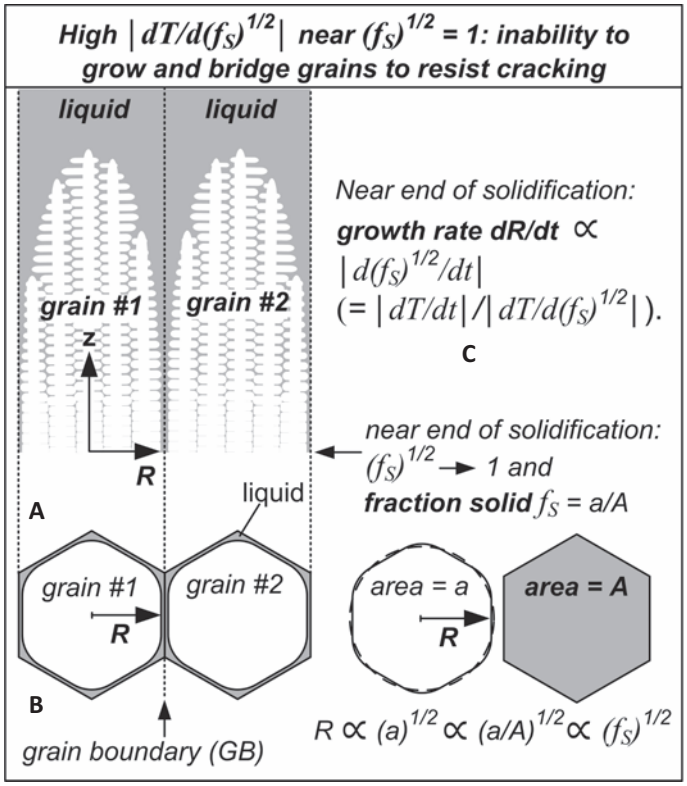

Fig. 4 — Lateral growth rate of grains. A — Longitudinal cross section; B — characteristic grain radius R *and transverse cross-section area* a *near end of solidification; C — growth rate* dR/dt *(*dT/dt *being cooling rate). In B,* R *is proportional to* $a^{1/2}$ *because* a *is nearly round, as shown by broken circles. Near end of solidification, liquid within grains is negligible as compared to solid, and so* f_S = a/A.

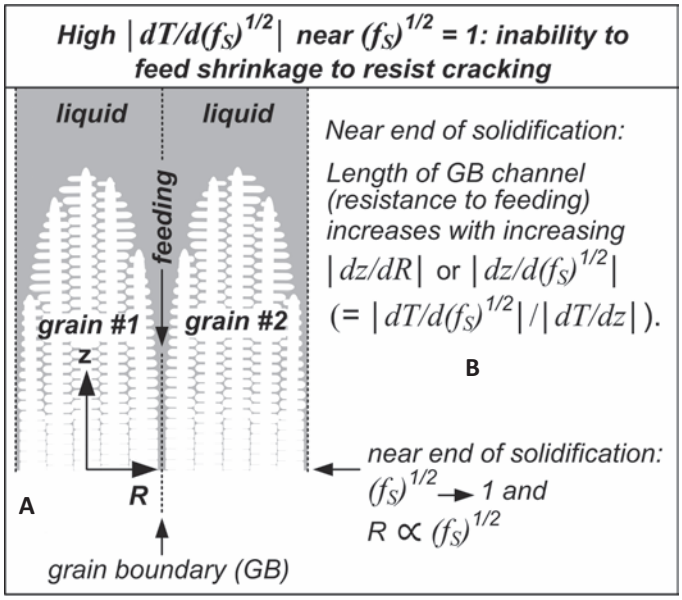

Fig. 5 — Liquid feeding along grain boundary to resist cracking. A — Longitudinal cross section; B — length of liquid channel. A large |dz/dR| *means* R *hardly increases as* z *decreases significantly, i.e., a long liquid channel between grains, which hinders the liquid feeding needed to resist cracking.* dT/dz *is axial temperature gradient.*

used as an index for the susceptibility to solidification cracking, that is, the steeper the slope of the $T–(f_S)^{1/2}$ curve near $(f_S)^{1/2}$ = 1 is, the greater the crack susceptibility.

Calculation of T-$(f_S)^{1/2}$ Curves and Crack Susceptibility Index

By using the relationship between T and f_S, the phase diagram is considered, including the alloy composition C_o, the equilibrium segregation ratio k, the liquidus-line slope m_L, and the freezing temperature range. Curves of T vs. $(f_S)^{1/2}$ were calculated using commercial thermodynamic software packages Pandat (Ref. 23) and Al database PanAluminum (Ref. 24). The simple Scheil solidification model (Ref. 2) was adopted, with a temperature-dependent k and m_L. The Scheil model works fine because its assumption of equilibrium at the S/L interface (Ref. 2) is reasonable for arc welding, where the mild cooling rate does not cause significant undercooling as in laser- or electron-beam welding. Furthermore, cracking occurs shortly after solidification starts (no time for solid diffusion), e.g., 5 to 7 s as measured in permanent-mold casting of Mg alloys (Refs. 25–27) and even shorter in arc welding. According to Flemings (Ref. 2), the extent of solid-state diffusion can be related to a parameter $\alpha = 4D_S t_f/(d^2)$, where D_S is the coefficient of diffusion in solid, t_f the solidification time, and d the secondary dendrite arm spacing. Diffusion is significant when $\alpha k > 0.1$. Typically, k is around 0.15 (0.125 for Al-Si and 0.170 for Al-Cu). Based on the data of the secondary dendrite arm spacing of Al alloys vs. the cooling rate (Ref. 2), the cooling rate is about 100°C/s with a typical secondary dendrite arm spacing of 1×10^{-5} m. As will be seen subsequently, the average freezing temperature range of 2014, 2024, 2219, 6061, and 7075 Al is about 125°C. Taking this as a typical solidification temperature range, the local freezing time t_f is about 1.25 s, that is, (125°C) / (100°C/s). If the diffusion coefficient in solid D_S is taken as 1×10^{-12} m^2/s, $\alpha = 4 \times (1 \times 10^{-12}$ $m^2/s) (1.25$ s) / $(1 \times 10^{-5}$ m$)^2$ = 0.05, and $\alpha k = 0.05 \times 0.15 = 0.0075$.

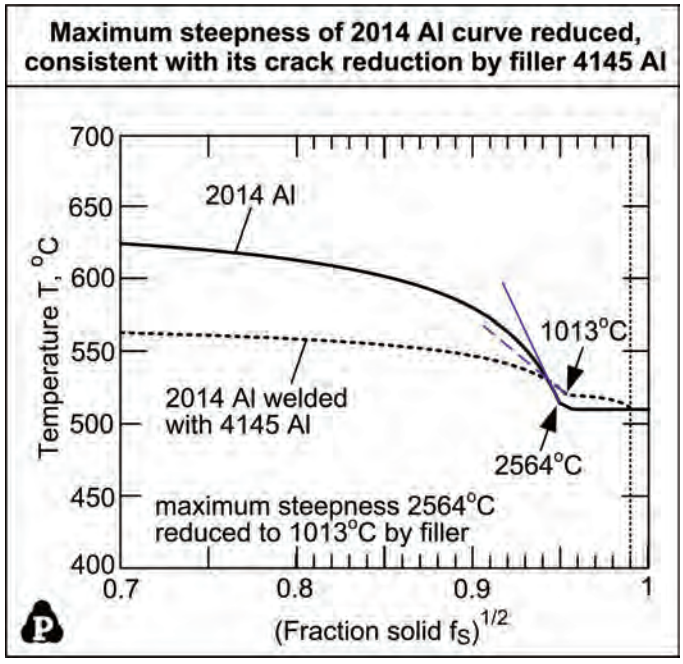

Fig. 6 — Maximum steepness $|dT/d(f_S)^{1/2}|$ of 2014 Al reduced by filler metal 4145 Al, consistent with its recommendation for reducing solidification cracking in 2014 Al (Refs. 29, 30). The weld consists of 20% 2014 and 80% 4145. (Beyond $(f_S)^{1/2} = 0.99$, too little liquid is assumed available to form continuous grain-boundary liquid films to cause cracking.) The straight lines are tangents to the curves at the locations of their maximum steepness.

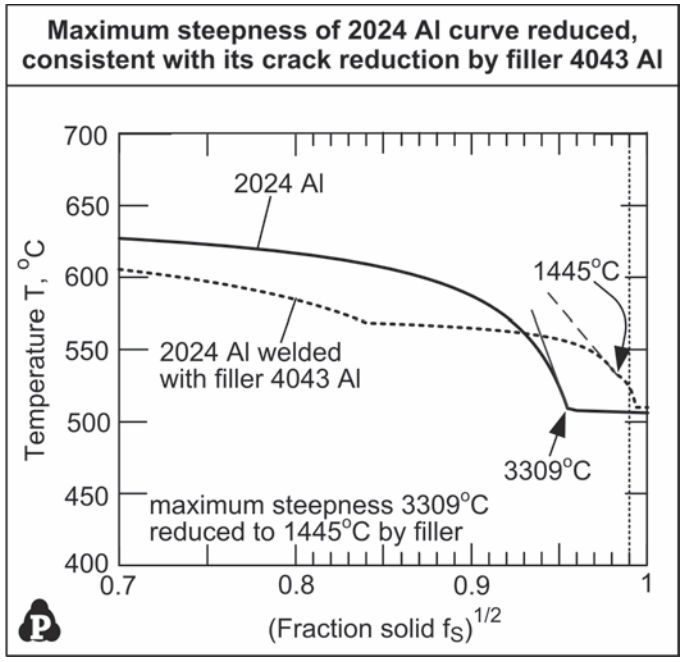

Fig. 7 — Maximum $|dT/d(f_S)^{1/2}|$ of 2024 Al reduced by filler metal 4043 Al, consistent with 4043 Al reducing cracking in crack susceptibility tests of 2024 Al (Refs. 31, 32). The weld consists of 20% 2024 and 80% 4043.

Since $ak < 0.1$, solid-state diffusion can be neglected and the Scheil solidification model can be used. However, with large k such as 0.48 for Al-Mg, diffusion can be significant.

In analyzing the crack susceptibility based on the T-$(f_S)^{1/2}$ curve, it will be assumed that the crack susceptibility is over at a point very close to $(f_S)^{1/2} = 1$. At this point there is no longer enough liquid left to form continuous liquid films to separate grains, and extensive bridging between grains can occur to resist solidification cracking. In the RDG model (Ref. 10), the crack susceptibility was assumed to end at $f_S = 0.98$, and in the model of Clyne and Davies (Ref. 9) at $f_S = 0.99$. It is more difficult to maintain continuous liquid films between grains to cause cracking with 1% liquid left ($f_S = 0.99$) than 2% ($f_S = 0.98$), keeping in mind that a portion of liquid exists within grains and it does not contribute to the formation of grain boundary liquid films. It is recognized that the f_S value corresponding to the end of crack susceptibility is not universal but is likely to depend on the alloy involved. For the purpose of discussion, however, this point is assumed to be $(f_S)^{1/2} = 0.99$, which corresponds to $f_S = 0.98$.

Furthermore, it will be assumed that the maximum steepness of the T-$(f_S)^{1/2}$ curves, which occurs near $(f_S)^{1/2} = 1$, can be used to represent the crack susceptibility index, which is $|dT/d(f_S^{1/2})|$ near $(f_S)^{1/2} = 1$. In other words, the maximum $|dT/d(f_S^{1/2})|$ of the T-$(f_S)^{1/2}$ curve will be calculated and used as the crack susceptibility index. If the maximum steepness occurs after $(f_S)^{1/2} = 0.99$, the steepness at $(f_S)^{1/2} = 0.99$ will be taken as the index.

In the previous study (Ref. 20), an average steepness $|\Delta T/\Delta(f_S^{1/2})|$ was taken over a range of $(f_S)^{1/2}$ close to 1.0 to represent the crack susceptibility. This required selecting a $(f_S)^{1/2}$ range and determining the corresponding temperature difference. It is believed that the maximum steepness is more naturally related to the crack susceptibility revealed by the T-$(f_S)^{1/2}$ curve. It is also more straightforward to determine. Thus, the maximum steepness will be used throughout the present study.

Effect of Filler Metals on Crack Susceptibility

The compositions of some commercial Al wrought alloys, filler metals, and welds are shown in Table 1 (Ref. 28). Filler metal 4043 Al can be used to reduce solidification cracking in several Al alloys (Refs. 29–32), but the strength of the resultant weld is low. Thus, new filler metals that are significantly stronger but still effective in reducing solidification cracking are desirable.

Figure 6 shows two $T\text{-}(f_S)^{1/2}$ curves. The one labeled with 2014 Al is for a weld made with a matching filler metal and the other one is for a weld made with commercial filler metal 4145 Al. In the former, a matching filler metal refers to a filler metal identical to the base metal in composition. The use of a matching filler metal is equivalent to welding without a filler metal, that is, autogenous welding. In the latter, the filler metal is diluted 20% by the base metal. That is, the weld consists of 80% 4145 Al and 20% 2014 Al (Ref. 1), and its composition is shown in Table 1.

As shown, the maximum steepness of the $T\text{-}(f_S)^{1/2}$ curve of 2014 Al is 2564°C, and it occurs at $(f_S)^{1/2} = 0.95$, which is close to 1.0. With filler metal 4145 Al, the maximum steepness of the $T\text{-}(f_S)^{1/2}$ curve of 2014 Al is reduced to 1013°C, which predicts a significant reduction in the crack susceptibility of 2014 Al by filler metal 4145 Al. This prediction is consistent with the recommendation of filler metal 4145 Al for reducing solidification cracking in welding 2014 Al (Refs. 29, 30).

The case of 2024 Al is shown in Fig. 7. The dilution of filler metal 4043 Al by the base metal is 20%. As shown, the maximum steepness of slope of the $T\text{-}(f_S)^{1/2}$ curve of 2024 Al is 3309°C at $(f_S)^{1/2} = 0.95$. This is reduced to 1445°C by filler metal 4043 Al, thus suggesting crack susceptibility reduction of 2024 Al by filler metal 4043 Al. This is consistent with the crack susceptibility tests that showed filler metal 4043 Al reduced solidification cracking in 2024 Al (Refs. 31, 32).

Figure 8 shows the case of 7075 Al. The dilution of filler metal 4043 Al by the base metal is 20%. The maximum steepness of slope of the $T\text{-}(f_S)^{1/2}$ curve of 7075 Al is 4152°C at $(f_S)^{1/2} =$

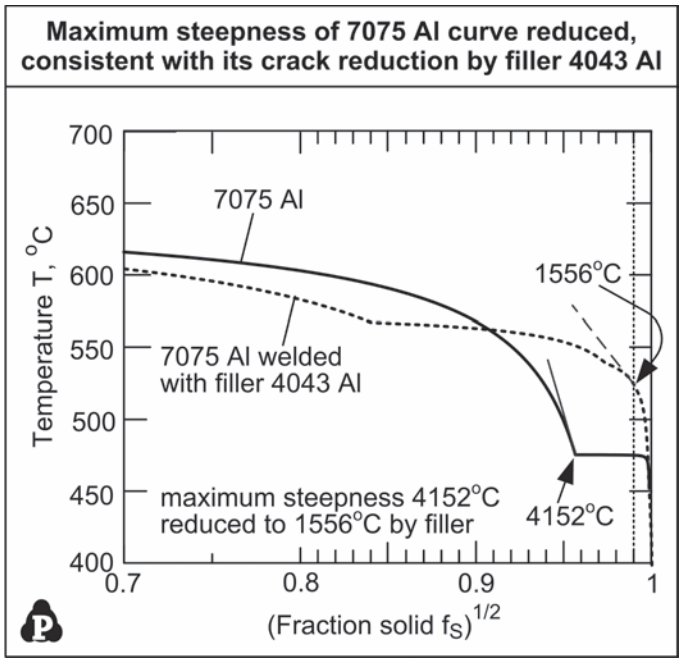

Fig. 8 — Maximum $|dT/d(f_S)^{1/2}|$ of 7075 Al reduced by filler metal 4043 Al, consistent with 4043 Al reducing cracking in crack susceptibility tests of 7075 Al (Refs. 31, 32). The weld consists of 20% 7075 and 80% 4043.

Table 1 — Compositions of Wrought Al Alloys, Filler Metals, and Welds in wt-% (Ref. 28)

	Si	Cu	Mn	Mg	Fe	Cr	Zn	Ti	Al
Workpiece									
2014	0.8	4.4	0.8	0.5	—	—	—	—	balance
2024	—	4.4	0.6	1.5	—	—	—	—	balance
2219	—	6.3	0.3	—	—	—	—	0.06	balance
6061	0.6	0.3	—	1.0	—	0.2	—	—	balance
7075	—	1.6	—	2.5	—	0.23	5.6	—	balance
5052	—	—	—	2.5	—	0.25	—	—	balance
5083	—	—	0.7	4.4	—	0.15	—	—	balance
Filler Metals									
4043	5.2	—			—				
4145	10	4.0							
5556	—	—	0.8	5.1	—	0.12	—	0.12	balance
Welds									
2014 with 80% 4145	0.8 x 0.2 + 10 x 0.8 = 8.16	4.4 x 0.2+ 4.0 x 0.8 = 4.08	0.8 x 0.2 = 0.16	0.5 x 0.2 = 0.10	—	—	—	—	balance
2024 with 80% 4043	5.2 x 0.8 = 4.16	4.4 x 0.2 = 0.88	0.6 x 0.2 = 0.12	1.5 x 0.2 = 0.3	—				balance
6061 with 80% 4043	0.6 x 0.2 + 5.2 x 0.8 = 4.28	0.3 x 0.2 = 0.06	—	1.0 x 0.2 = 0.2	—	0.2 x 0.2 = 0.04	—	—	balance
7075 with 80% 4043	5.2 x 0.8 = 4.16	1.6 x 0.2 = 0.32	—	2.5 x 0.2 = 0.5	—	0.23 x 0.2 = 0.046	5.6 x 0.2 = 1.12	—	balance
5052 with 80% 5556	—	—	0.8 x 0.8 = 0.64	2.5 x 0.2+ 5.1 x 0.8 = 4.58	—	0.25 x 0.2 + 0.12 x 0.8 = 0.146	—	0.12 x 0.8 = 0.096	balance

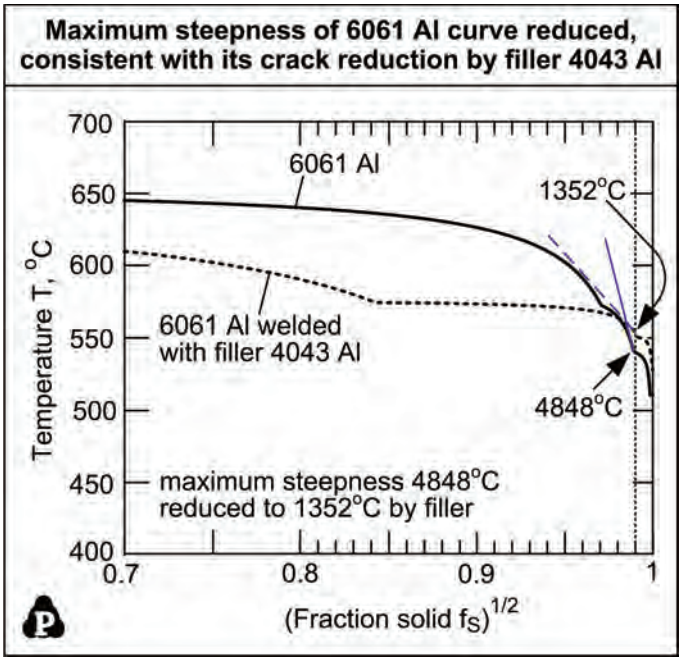

Fig. 9 — Maximum $|dT/d(f_S)^{1/2}|$ of 6061 Al reduced by filler metal 4043 Al, consistent with its recommendation for reducing solidification cracking in 6061 Al (Refs. 29, 30). The weld consists of 20% 6061 and 80% 4043.

0.95. As mentioned previously, beyond $(f_S)^{1/2} = 0.99$, there is probably too little liquid left at the grain boundary to cause solidification cracking. As shown, filler metal 4043 Al reduces this maximum steepness to 1556°C, thus it can be expected to reduce the crack susceptibility of 7075 Al. This is consistent with the crack susceptibility tests that showed filler metal 4043 Al reduced solidification cracking in 7075 Al (Refs. 31, 32).

The case of 6061 Al is shown in Fig. 9. The filler metal 4043 Al is diluted 20% by the base metal. The maximum steepness $|dT/d(f_S^{1/2})|$ of the $T–(f_S)^{1/2}$ curve is 4848°C and is at $(f_S)^{1/2} = 0.99$. Unlike previous cases, the high steepness portion of the curve covers a wider $(f_S)^{1/2}$ range, say about 0.95 to 0.99. The maximum steepness is reduced by filler metal 4043 Al to 1352°C, suggesting the crack susceptibility of 6061 Al can be reduced significantly by 4043 Al. This is consistent with the recommendation of filler metal 4043 Al for reducing solidification cracking in welding 6061 Al (Refs. 29, 30). It is also consistent with the experimental results of Coniglio and Cross (Refs. 12, 13) that showed the critical strain rate needed to cause cracking increased when 4043 Al was used to weld 6061 Al alloy.

The proposed crack susceptibility index can be used to guide the selection of filler metals, including the proper dilution level needed, to resist solidification cracking. As filler metals resistant to solidification cracking are often weak, the index may also help guide the search for new filler metals that can make welds stronger. Published guides for existing filler metals (Refs. 29, 30) do not show the effect of filler-metal dilution by the base metal on the crack susceptibility. To show the effect, a series of $T–(f_S)^{1/2}$ curves can be calculated at various levels of dilution. The index may also be useful for computer modeling of solidification cracking in welding.

The freezing temperature range sometimes correlates well with the susceptibility to solidification cracking (Ref. 1), that is, the temperature range from the beginning ($f_S = 0$) of solidification to the end ($f_S = 1$). Table 2 shows the freezing temperature ranges of alloys 2014, 2024, 7075, and 6061, welded without and with filler metals, calculated using Pandat (Ref. 23) and PanAluminum (Ref. 24) based on the Scheil solidification model. As shown, significant reduction in the freezing temperature range is observed in the cases of 2014 Al and 6061 Al, but not in the cases of 2024 Al and 7075 Al, even though significant reduction has been observed in practice in each case.

Crack Susceptibility of Al Wrought Alloys

An attempt will now be made to compare the crack susceptibility of the aforementioned Al wrought alloys welded either without any filler metals or with matching filler metals. The $T-(f_S)^{1/2}$ curves of 2219, 2014, 2024, 7075, and 6061 Al alloys are shown in part in Fig. 10. As mentioned previously, beyond $(f_S)^{1/2} = 0.99$ there is probably too little liquid left at the grain boundary to form a continuous

Table 2 — Freezing Temperature Ranges of Some Wrought Alloys Welded without and with Filler Metals

Alloy	2014 Al	2024 Al	7075 Al	6061 Al
Filler metal	4145 Al	4043 Al	4043 Al	4043 Al
Freezing temperature range of weld made without filler metal	640°C (f_s = 0) – 511°C (f_s = 1) = 129°C	640°C (f_s = 0) – 507°C (f_s = 1) = 133°C	634°C (f_s =0) – 455°C (f_s =1) = 179°C	652°C (f_s = 0) – 511°C (f_s = 1) = 141°C
Freezing temperature range of weld made with 80% filler metal	594°C (f_s = 0) – 511°C (f_s = 1) = 83°C	631°C (f_s = 0) – 507°C (f_s = 1) = 120°C	630°C (f_s=0) – 390°C (f_s=1) = 240°C	634°C (f_s=0) – 529°C (f_s=1) = 105°C
Reduction in freezing temperature range caused by filler metal	46°C	13°C	- 61°C	36°C

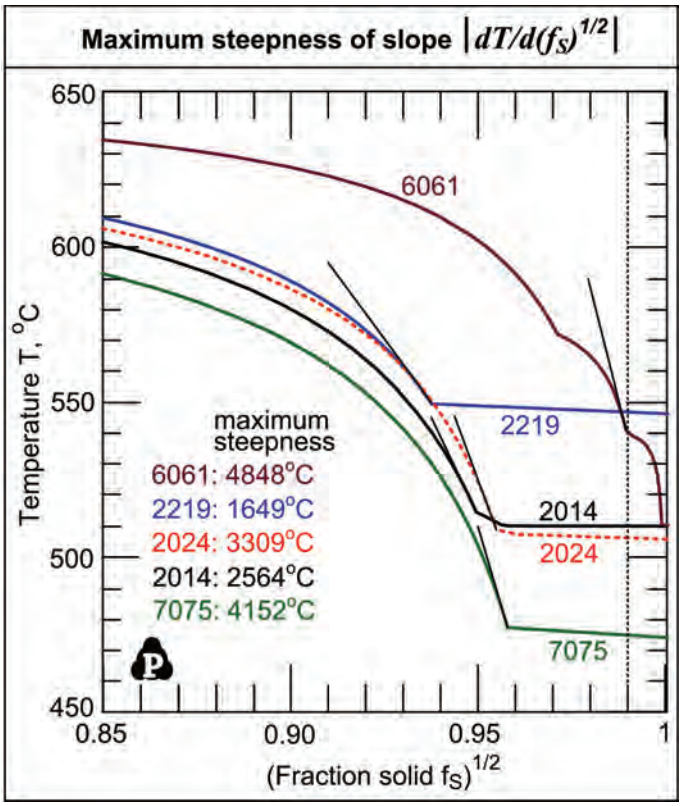

Fig. 10 — T-$(f_S)^{1/2}$ curves of the aforementioned Al alloys showing the maximum steepness of the slopes of the curves. As the maximum steepness is approached, $(f_S)^{1/2}$ increases (grains grow) much more slowly as T drops and tensile strain rises, thus prolonging the liquid (vulnerable) state of grain boundaries.

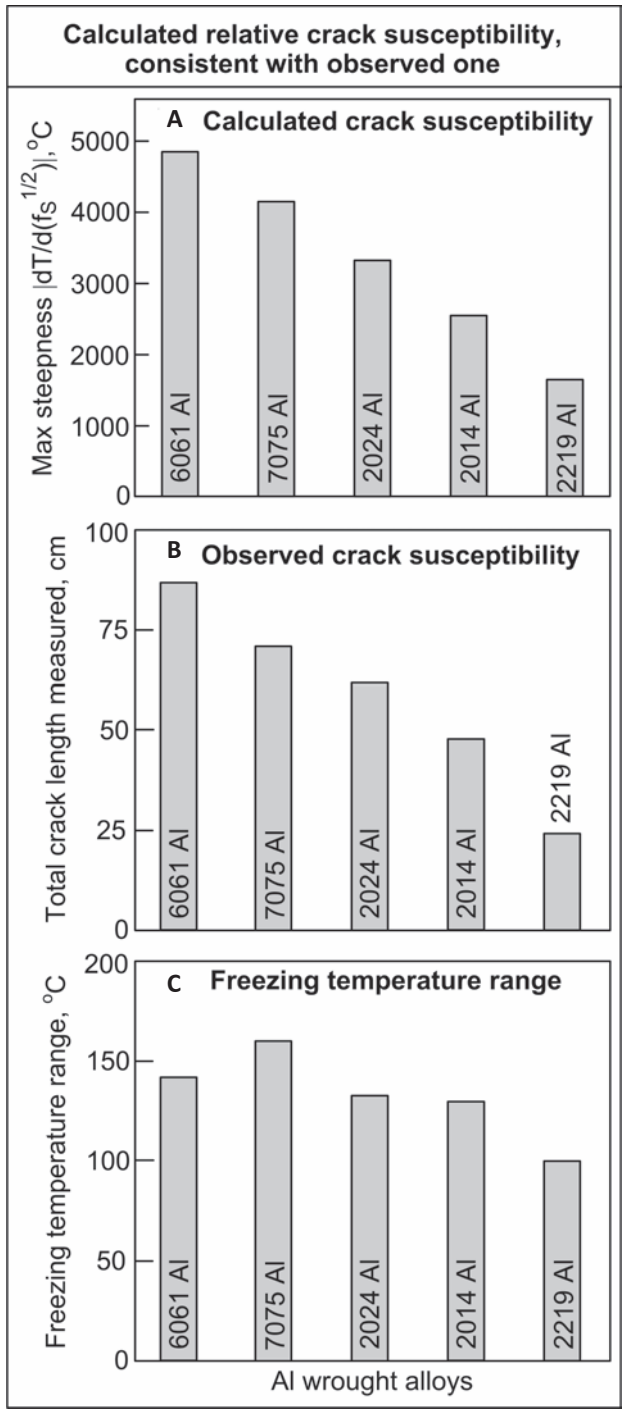

Fig. 11 — Susceptibility of the aforementioned Al alloys to solidification cracking. A — Calculated results based on maximum steepness of T-$(f_S)^{1/2}$ curves in Fig. 10; B — experimental results from crack-susceptibility tests (Refs. 31, 32); C — freezing temperature range showing no close correlation with observed crack susceptibility.

film to promote solidification cracking. As shown, the maximum steepness of the slope of the curve increases in the order of 2219, 2014, 2024, 7075, and 6061.

In Fig. 11A, the crack susceptibility of the aforementioned alloys is ranked based on the maximum steepness of the T-$(f_S)^{1/2}$ curve. The maximum steepness is lowest with 2219 Al, which is known to have good weldability, and highest with 7075 Al and 6061 Al, which are known for their very high susceptibility to solidification cracking. The reported experimental data are shown in Fig. 11B, expressed in terms of the crack lengths measured in crack susceptibility tests (Refs. 31, 32). The agreement between the calculated crack susceptibility and the reported one is surprisingly good. The T-$(f_S)^{1/2}$ curves in Fig. 10 show that the narrower grain boundary channel of 6061 Al may contribute to its higher crack susceptibility through hindering liquid feeding. The freezing temperature ranges of the alloys, calculated using Pandat (Ref. 23) and PanAluminum (Ref. 24) based on the Scheil model, are shown in Fig. 11C. They do not correlate well with observed crack susceptibility data.

T-$(f_S)^{1/2}$ Curves and Liquid Channel

In Fig. 12, the liquid/grain interfaces near the grain boundaries are shown by the T-$(f_S)^{1/2}$ curves for Al wrought alloys 2219 Al and 6061 Al. A liquid/grain interface near the grain boundary of an alloy can be represented by its T-$(f_S)^{1/2}$ curve because temperature is proportional to the axial distance z (assuming constant temperature gradient dT/dz) and $(f_S)^{1/2}$ to the radial distance R near $(f_S)^{1/2} = 1$ (the GB).

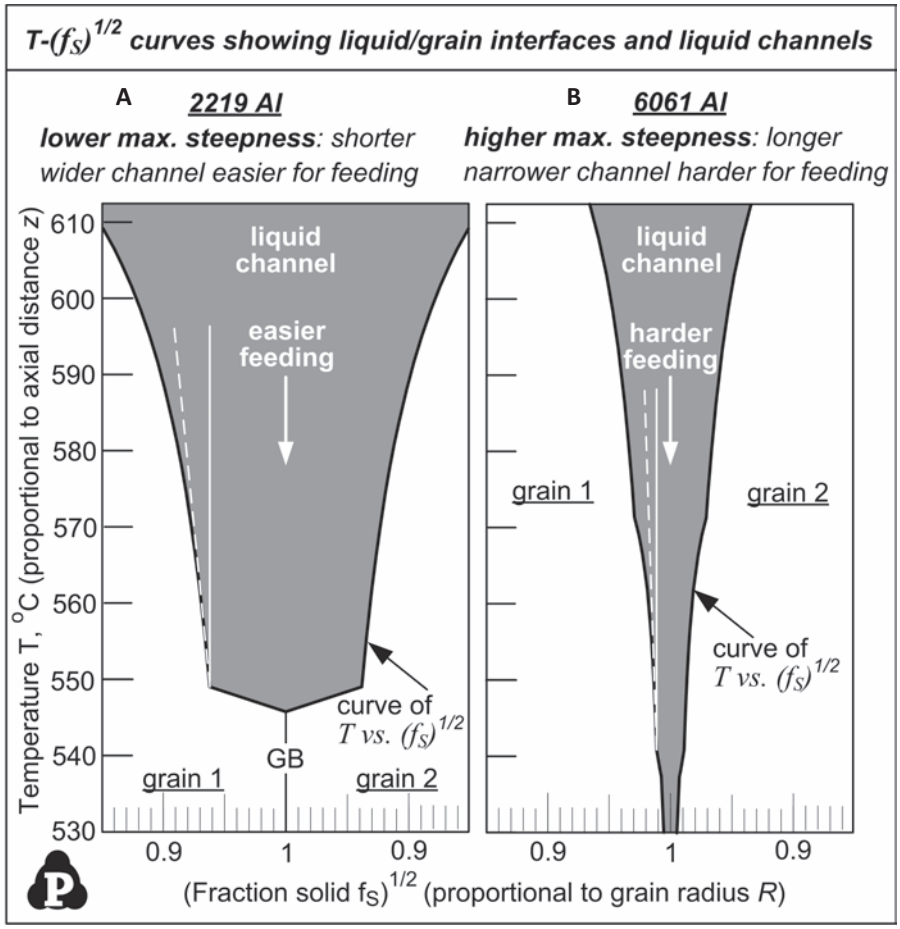

Fig. 12 — T-(f_S)$^{1/2}$ curves showing liquid/grain interfaces, liquid channels and tangents to curves at locations of maximum steepness. A — 2219 Al alloy; B — 6061 Al alloy. A longer, narrower channel hinders liquid feeding because of the resistance to flow caused by the viscosity of liquid.

The slope of the curve is $dT/d(f_S^{1/2})$ and the steepness of the slope is thus $|dT/d(f_S^{1/2})|$. In the case of 6061 Al to the maximum steepness of its T-$(f_S)^{1/2}$ curve is higher and the grain boundary channel is longer and narrower. As mentioned previously (Fig. 5), according to the Hagen-Poiseuille law (Ref. 22), the volumetric flow rate of a liquid through a channel decreases with increasing channel length and decreasing channel opening due to the resistance to flow caused by the viscosity of the liquid. Thus, liquid feeding can be expected to be more difficult with 6061 Al. It is perhaps worth mentioning that liquid feeding occurs all the way to the end of the grain boundary channel, where the liquid is sucked toward the end to feed the shrinkage caused by the solidification of the last liquid.

T-$(f_S)^{1/2}$ Curves and Theories of Cracking

As the workpiece and the mushy zone cool and contract during welding, the tensile strain and stress they induce in the mushy zone continue to rise. As can be seen in Fig. 10, as the location of the maximum steepness of the T-$(f_S)^{1/2}$ curve is approached, temperature T continues to drop (and induce more strain and stress), but $(f_S)^{1/2}$ must now increase much more slowly because the steepness $|dT/d(f_S^{1/2})|$ increases significantly. This significantly prolongs the time for the grain boundary to remain in the liquid, and hence, vulnerable state while temperature is dropping and tensile strain or stress is rising. The higher the maximum steepness of the T-$(f_S)^{1/2}$ curve is, the greater the chance of exceeding the tolerable limit of strain or stress before $(f_S)^{1/2}$ reaches the level needed to bond together and resist cracking, for instance, 0.99.

This concept of the maximum steepness of the T-$(f_S)^{1/2}$ curve may be integrated with existing theories of solidification cracking or hot tearing. Suppose an ordinary strain- or stress-based theory is being considered. Cracking can occur if the tensile strain or stress in the mushy zone exceeds the tolerable limit before grains bond together. Suppose the strain theory of Pellini (Ref. 6) instead is being considered. Cracking can occur if the highly localized strain in the liquid films between neighboring grains exceeds the tolerable limit before grains bond together. According to the theory, longer-existing liquid films provide a greater chance for the strain in them to exceed the critical limit and cause them to fracture, that is, cause cracking. This is consistent with the concept of the maximum steepness.

If a strain-rate-based theory is being considered, Equation 5 can be applied. As the maximum steepness is approached, $|dT/d(f_S^{1/2})|$ can increase significantly, that is, $|d(f_S)^{1/2}/dT|$, and hence, the RHS of Equation 5 can decrease significantly. When the RHS becomes small enough to be exceeded by the LHS of the equation, cracking can occur. Similarly, if Prokhorov's model (Ref. 7) is being considered, Equation 6 can be applied. Again, as the maximum steepness of the T-$(f_S)^{1/2}$ curve is approached, $|d(f_S)^{1/2}/dT|$ and hence the RHS of Equation 6 can decrease significantly. Cracking can occur when the RHS is exceeded by the LHS. Thus, the concept of the maximum steepness of the T-$(f_S)^{1/2}$ curve can be integrated into most existing theories of solidification cracking or hot tearing.

Crack Susceptibility of Binary Al Alloys

An attempt will also be made to find the most crack susceptible compositions of binary Al-Si, Al-Cu, and Al-Mg alloys. Again, this will be done based on the maximum steepness of the T-$(f_S)^{1/2}$ curve. The crack susceptibility of binary Al-Si, Al-Cu, and Al-Mg alloys as a function of composition has

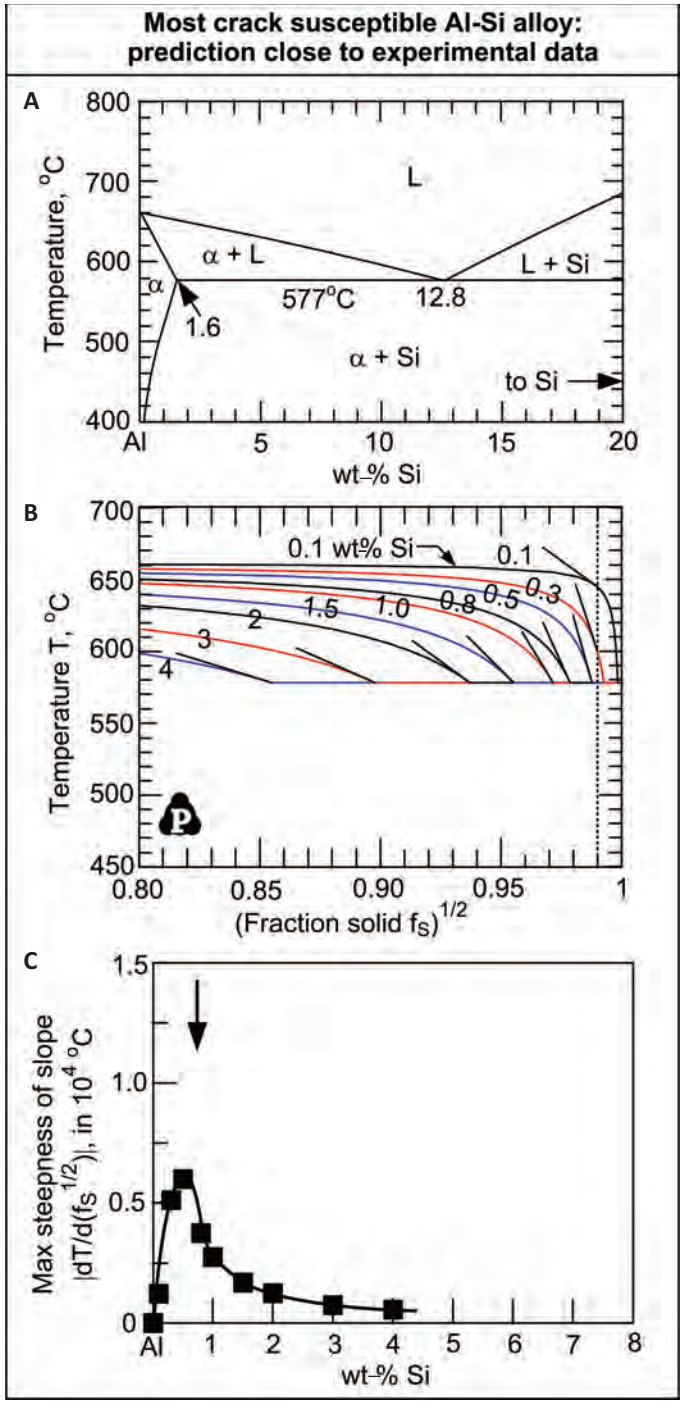

Fig. 13 — Binary Al-Si alloys. A — Phase diagram (Ref. 40); B — curves of T-$(f_S)^{1/2}$; C — calculated maximum crack susceptibility at 0.5 wt-% Si, which is close to that at 0.8 wt-% Si reported by Singer et al. (Ref. 33).

been investigated in casting and welding. A peak crack susceptibility at about 0.8 wt-% Si was reported by Singer et al. (Ref. 33) in casting Al-Si alloys. In the case of Al-Mg alloys, a peak crack susceptibility at about 5 wt-% Mg was observed by Rosenbergh et al. (Ref. 34) in casting. A peak at around 1.75 wt-% Mg was also reported, including Dowd et al. (Ref. 31) at about 1.5 wt-% Mg in arc welding and Cross et al. (Ref. 35) at about 2 wt-% Mg in arc welding (Varestraint testing of cast alloys). As for Al-Cu alloys, a peak around 1 wt-% Cu has been reported, including 1 wt-% Cu by Novikov et al. (Ref. 36) in casting and 1 wt-% Cu by Spittle et al. (Ref. 37) in casting. A peak around 3 wt-% Cu has also been reported, including 3 wt-% Cu by Pumphrey and Lyons (Ref. 38) in casting, about 3 wt-% Cu by Cross et al. (Ref. 35) in arc welding (Varestraint testing of cast alloys), and about 3.5 wt-% Cu by Michaud et al. (Ref. 39) in laser welding. Rosenberg et al. (Ref. 34) observed a peak at about 5 wt-% Cu in casting.

Figure 13 shows the case of the binary Al-Si alloys. For convenience of discussion, the binary Al-Si phase diagram is included (Fig. 13A) (Ref. 40). The T-$(f_S)^{1/2}$ curves are shown for Al-Si alloys of various Si contents (Fig. 13B). They show a relatively short freezing temperature range and a very large amount of eutectic liquid, which solidifies isothermally at the end of solidification. The shallow steepness $|dT/d(f_S^{1/2})|$ suggests fast growth of grains toward each other to bond together to resist cracking and a short wide liquid channel along the grain boundary easy for liquid feeding to resist cracking. Figure 13C shows the calculated crack susceptibility curve as a function of the Si content. The curve shows a calculated peak crack susceptibility of 6 ¥ 10³°C at 0.5 wt-% Si, which is close to that of about the 0.8 wt-% Si observed by Singer et al. (Ref. 33).

The case of binary Al-Cu alloys is shown in Fig. 14 along with the phase diagram (Ref. 40). As compared to binary Al-Si alloys, they show a wider freezing temperature range and a much smaller amount of eutectic liquid at the end of solidification. The calculated crack susceptibility curve shows a peak crack susceptibility of 1.0 ¥ 10⁴°C at 1.5 wt-% Cu. This peak is between that at about 1 wt-% Cu observed by Novikov et al. (Ref. 36) and Spittle et al. (Ref. 37) and that at about 3 wt-% Cu observed to Pumphrey et al. (Ref. 38), Cross et al. (Ref. 35), and Michaud et al. (Ref. 39).

The case of binary Al-Mg alloys is shown in Fig. 15 along with the phase diagram (Ref. 40). They show a much wider freezing temperature range and a smaller amount of eutectic liquid at the end of solidification than binary Al-Si and Al-Cu alloys. The calculated crack susceptibility curve shows a peak crack susceptibility of 1.26 ¥ 10⁴°C at 3 wt-% Mg, which lies between that of about 1.75 wt-% Mg observed by

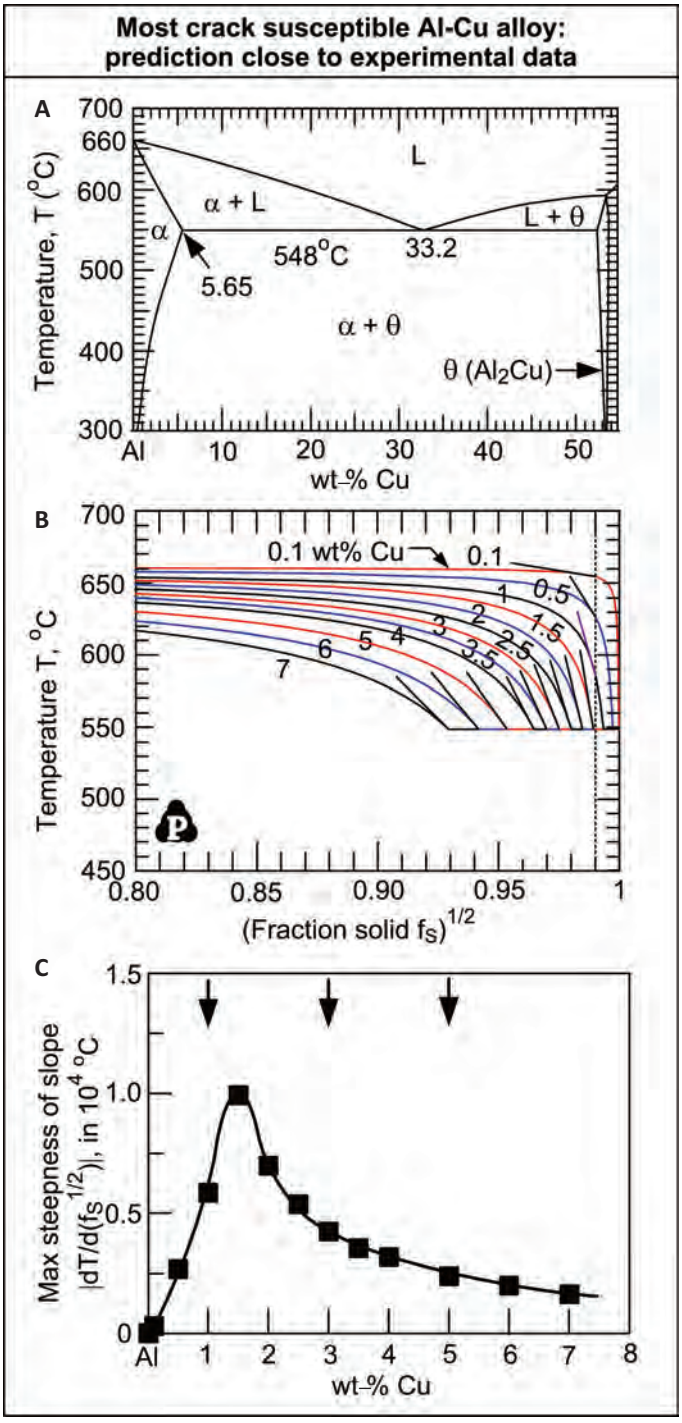

Fig. 14 — Binary Al-Cu alloys. A — Phase diagram (Ref. 40); B — curves of $T\text{-}(f_S)^{1/2}$*; C — calculated crack susceptibility curve showing a peak at 1.5 wt-% Cu, between that reported by Novikov et al. (Ref. 36) and Spittle et al. (Ref. 37) and that by Pumphrey et al. (Ref. 38), Cross et al. (Ref. 35), and Michaud et al. (Ref. 39). Diffusion may have caused the 5 wt-% peak.*

Dowd et al. (Ref. 31) and Cross et al. (Ref. 35) and that of 5 wt-% Mg reported by Rosenberg et al. (Ref. 34).

Thus, the crack susceptibility curves of binary Al-Si, Al-Cu, and Al-Mg alloys as a function of the solute content can be calculated with good agreement with the compositions of the most crack susceptible alloys observed in crack susceptibility tests. However, the curves can be sensitive to the selection of the point of extensive bridging to end the crack susceptibility. Overall speaking, $(f_S)^{1/2}$ = 0.99 seems to result in good agreement with the most crack-susceptible binary alloys observed in crack-susceptibility tests.

As can be seen by comparing Figs. 14C and 15C, the calculated peak crack susceptibility of binary Al-Mg alloys 1.26 ¥ 10⁴°C is significantly higher than that of Al-Cu alloys 1.0 ¥ 10⁴°C. The very wide freezing temperature of Al-Mg alloys contributes to their steep $T\text{-}(f_S)^{1/2}$ curves near $(f_S)^{1/2}$ = 1, and hence, maximum $|dT/d(f_S)^{1/2}|$. In reality, in spite of its very wide freezing temperature, the crack susceptibility of 5083 Al (~Al-4.4Mg) is mild, somewhat higher (Refs. 31, 32) or less than (Ref. 41) that of 2219 Al (~Al-6.3Cu). This discrepancy is likely caused by the use of the Scheil solidification model, which neglects solid-state diffusion.

As can be seen in Fig. 15A, the Al-Mg phase diagram has a very high maximum solid solubility, C_{SM}, of 17.5 wt-% Mg. For comparison, C_{SM} is 1.6 wt-% Si for Al-Si alloys (Fig. 13A) and 5.65 wt-% Cu for Al-Cu alloys (Fig. 14A). With a very low C_{SM}, little solute can diffuse into the Al-rich dendrites during solidification even with a long diffusion time and a high diffusion coefficient. Contrarily, with a very high solid solubility, much more solute can diffuse into the dendrites even with a normal diffusion time and diffusion coefficient. With a significant amount of Mg diffusing into Al-rich dendrites, however, the Mg content of the interdendritic liquid at a given temperature T can fall below that dictated by the phase diagram unless f_S increases significantly to reject more Mg into the liquid. Thus, f_S is increased at a given T and this makes the $T\text{-}(f_S)^{1/2}$ curve significantly shallower and hence the steepness $|dT/d(f_S)^{1/2}|$ significantly lower. Thus, the proposed crack susceptibility index $|dT/d(f_S)^{1/2}|$ can still be consistent with the relatively low crack susceptibility of Al-Mg alloys by calculating $|dT/d(f_S)^{1/2}|$ using a solidification model that considers diffusion instead of the Scheil equation (Ref. 42).

The relatively large dihedral angle of Al-Mg alloys may also contribute to

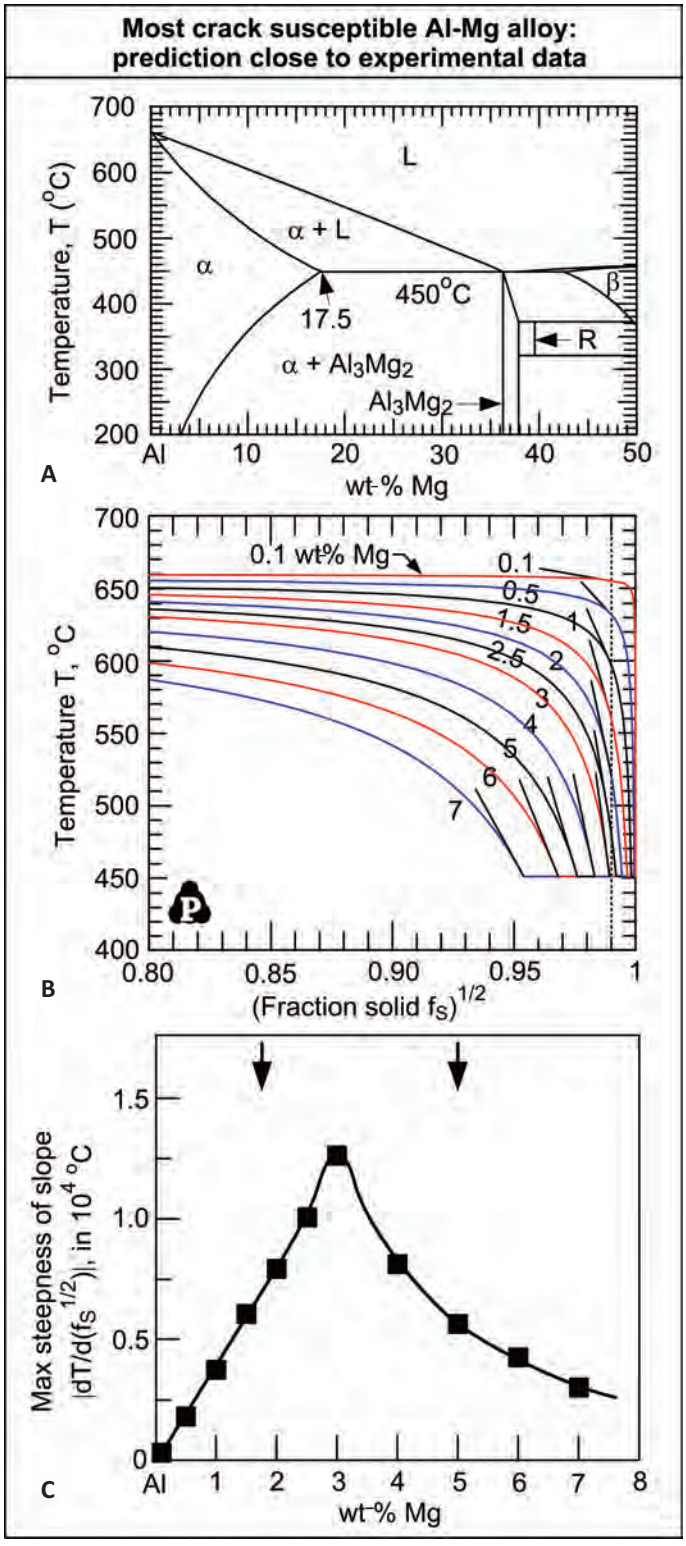

Fig. 15 — Binary Al-Mg alloys. A — Al-Mg phase diagram (Ref. 40); B — curves of $T\text{-}(f_S)^{1/2}$*; C — calculated crack susceptibility curve showing a peak at 3 wt-% Mg, between that reported by Dowd et al (Ref. 31) and Cross et al. (Ref. 35) and that by Rosenberg et al. (Ref. 34).*

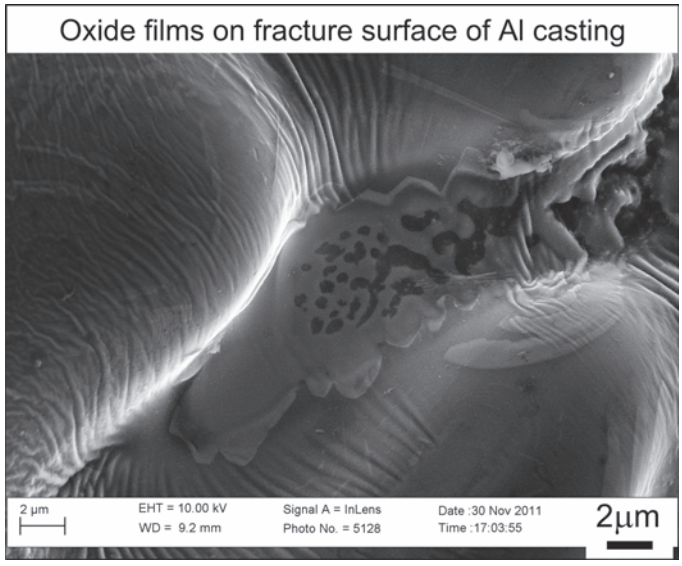

Fig. 16 — Fracture surface of an Al alloy that cracked during solidification in casting, suggesting oxide films acted as a crack initiation site (Ref. 46). The alloy is A206 (~Al-4.86Cu) containing 1 wt-% Al_2O_3 *nanoparticles. Oxide films can be easily introduced into liquid Al during shape and ingot casting to provide crack initiation sites during weld pool solidification.*

their relatively low crack susceptibility. The dihedral angle (Ref. 43), related to the surface tension of the interdendritic liquid, is an angle associated with the thinness or sharpness of the liquid at grain boundaries. A higher dihedral angle is likely to be associated with greater resistance to solidification cracking because the grain boundary liquid is less likely to form very thin continuous films to separate grains (Ref. 1). It has been reported that the dihedral angle of the grain boundary eutectic after solidification is 65 deg for 5083 Al, as compared to the 20 deg of 2219 Al (Ref. 41). Arata et al (Ref. 44) observed higher dihedral angles in binary Al-Mg alloys than binary Al-Cu alloys, for instance, 53 deg in Al-4.88Mg as compared to 20 deg in Al-6.32Cu.

Besides the dihedral angle, the proposed index has not considered the formation of secondary phases during solidification, which may also affect the crack susceptibility. For example, some intermetallic compounds can affect solidification cracking by bridging growing grains and/or blocking liquid feeding (Ref. 45).

Crack Nucleation Sites

As mentioned previously, the proposed criterion represents the necessary condition for cracking to occur during solidification, not the sufficient condition. To be sufficient, preexisting nucleation sites for cracks must be available (Ref. 21). The fact that the proposed index is able to predict the effect of the Al filler metals on the crack susceptibility of Al alloys seems to suggest similar preexisting nucleation sites may exist in various Al alloys.

Coniglio and Cross (Ref. 13) indicated that liquid metals may contain microsized pores that cannot escape during processing because of their limited buoyancy. They also indicated that metastable pore nuclei may also take the form of folded oxide films or gas trapped at the apex of oxides. According

to Campbell (Refs. 3, 4), oxides can exist in the form of folded films (called "bifilms") to initiate cracks during solidification. As explained by Campbell, when an Al melt is poured into the mold (in both shape casting and direct-chill casting of ingots), oxide films can be easily introduced unintentionally into the melt. Because of the very strong tendency of Al to oxidize in air, oxide films formed immediately on the liquid-stream surface and the free surface are carried into the inside of the melt by the action of pouring. Thus, oxide films can be expected to exist in solid Al because they already exist in liquid Al before solidification during shape and ingot casting.

Figure 16 shows an example of oxide films entrapped during casting acting as nucleation sites for cracking during solidification (Ref. 46). The oxide films on the fracture surface can be seen clearly. If they had formed by oxidation of the fracture surface after cracking had occurred, they would have no wrinkles. The A206 Al (~Al-4.86Cu) casting was prepared at UW-Madison by "constrained-rod casting" in a steel mold, in which cast rods were anchored at both ends to prevent shrinking and induce tension and hence cracking during solidification, similar to a "dog-bone" configuration. A small amount (about 1 wt-%) of Al_2O_3 nano particles was added to and dispersed in the melt in order to cast an A206 alloy containing Al_2O_3 nano particles. During the preparation of the melt for casting, oxide films were unavoidably entrapped in the melt as folded oxide films before casting.

In welding, the oxide films already present in a solid Al alloy can enter the weld pool. Under the action of strong convection caused by the Lorentz force, surface-tension force, and the momentum of the impinging filler-metal droplets (Ref. 1), the oxide films in the weld pool can break up into small pieces and act as nucleation sites for crack initiation during solidification of the weld metal. If crack initiation occurs at the surface of the weld, however, no oxide films or micropores are needed (Ref. 21).

Conclusions

1) The maximum steepness of the slope of the T-$(f_S)^{1/2}$ curve, $|dT/d(f_S)^{1/2}|$, has been proposed as a simple index for the susceptibility of an alloy to solidification cracking. It is based on a recent solidification cracking criterion that considers basic factors such as the phase diagram, solidification shrinkage, strain rate, cooling rate, and liquid feeding. However, other factors may also affect the crack susceptibility, e.g., the dihedral angle and secondary phases.

2) The index has been calculated for Al alloys using the Scheil solidification model of no solid-state diffusion, though other models with solid-state diffusion can also be used if available.

3) Several critical predictions for Al alloys based on the proposed index have been verified, including the crack susceptibility reduction by commercial Al filler metals, the relative crack susceptibility of wrought Al alloys 2014, 2024, 2219, 6061, and 7075, and the most crack susceptible compositions of binary Al-Si, Al-Cu, and Al-Mg alloys.

4) The predicted crack susceptibility of Al-Mg alloys is too high. However, this is not because of the index itself but because of the use of the Scheil solidification model to calculate the index. The model neglects Mg diffusion into Al-rich dendrites, which can be unusually significant because of the very high Mg solubility in solid Al. The use of a solidification model that allows solid-state diffusion is expected to reduce $|dT/d(f_S)^{1/2}|$, consistent with the relatively low crack susceptibility of Al-Mg alloys.

5) The index can be used as a guide to the selection of existing Al filler metals or the search for new ones to resist solidification cracking in welding. The index is easy to use as the curves of T vs. $(f_S)^{1/2}$ can be plotted easily using commercial thermodynamic software packages and databases. The effect of the filler-metal dilution by the base metal on the crack susceptibility, which is not shown in published guides, can be analyzed with the help of the proposed index.

6) The fact that the proposed index is consistent with the crack susceptibility of many Al alloys in welding (and casting) seems to imply that the nucleation sites needed for crack initiation are readily available, perhaps provided by oxide films (which form immediately on liquid Al and which are easily entrapped in it during casting) or the weld surface.

Acknowledgments

The author would like to dedicate this paper to the late Professor Y. Austin Chang of the University of Wisconsin-Madison, who founded CompuTherm, LLC, and who was a former adviser, colleague, and friend of the author at the University of Wisconsin. The insightful and valuable comments made by Dr. John Campbell, Emeritus Professor of the University of Birmingham, UK, are deeply appreciated. For the application of solidification and transport phenomena to cracking during solidification, the author would like to thank his PhD advisor, Professor Merton C. Flemings of MIT, from whom he learned both subjects. He would also like to thank CompuTherm, LLC, Madison, Wis., for kindly providing Pandat 2014 and PanAluminum 2014 for calculating the T-$(f_S)^{1/2}$ curves, and his visiting graduate student, Chiangwei Liu, for providing the 6061 Al weld. This work was supported by the National Science Foundation under Grant No. DMR 1500367.

References

1. Kou, S. 2003. *Welding Metallurgy*, 2nd edition. Hoboken, N.J.: John Wiley and Sons, pp. 257–300.

2. Flemings, M. C. 1974. *Solidification Processing*, New York: McGraw-Hill, 252–256: Appendix B.

3. Campbell, J. 2003. *Castings*, second edition, Oxford: Butterworth Heinemann, pp. 216–247.

4. Campbell, J. 2015. *Complete Casting Handbook*, 2nd ed. Oxford: Butterworth Heinemann, pp. 21–30 and 444, 445.

5. Eskin, D. G., Suitno, K. L., and Katergman, L. 2004. Mechanical properties in the semi-solid state and hot tearing of aluminum alloys. *Prog Mater Sci* 49: 629–711.

6. Apblett, W. R., and Pellini, W. S. 1954. Factors which influence weld hot cracking. *Welding Journal* 33(2): 83-s to 90-s.

7. Prokhorov, N. N. 1962. Resistance to hot tearing of cast metals during solidification. *Russian Castings Prod.* (4): 172–175.

8. Feurer, U. 1977. Influence of Alloy composition and solidification conditions on dendrite arm spacing, feeding and hot tearing properties of aluminum alloys.

Quality Control of Engineering Alloys and the Role of Metals Science, Proceedings of the International Conference, Delf University of Technology, pp. 131–145.

9. Clyne, T. W., and Davies, G. J. 1981. Influence of composition on solidification cracking susceptibility in binary alloy systems. *British Foundryman* 74(4): 65–73.

10. Rappaz, M., Drezet, J. M., and Gremaud, M. 1999. A new hot-tearing criterion. *Metallurgical and Materials Transactions* (30A): 449–455.

11. Drezet, J. M., and Allehaux, D. 2008. Application of the Rappaz-Drezet-Gremaud hot tearing criterion to welding aluminum alloys. *Hot Cracking Phenomena in Welds II*, edited by Th. Bollinghaus, H. Herold, C. E. Cross, and J. C. Lippold. Springer: 19–37.

12. Coniglio, N., Cross, C. E., Michael, T., and Lammers, M. 2008. Defining a critical weld dilution to avoid solidification cracking in aluminum. *Welding Journal* (87): 237-s to 247-s.

13. Coniglio, N., and Cross, C. E. 2009. Mechanisms for solidification crack initiation and growth in aluminum welding. *Metallurgical and Materials Transactions* A (40A): 2718–2728.

14. Matsuda, F., Nakagawa, H., Nakada K., and Okada, H. 1979. The VDR cracking test for solidification cracking susceptibility of weld metals and its application to aluminum alloys. *Transactions of JWRI* 8: 85–95.

15. Matsuda, F., Nakata, K., Tsukamoto, K., and Uchiyama, T. 1984. Effect of additional element on weld solidification crack susceptibility of Al-Zn-Mg alloy (Report III). *Transaction of JWRI* (13): 57–66.

16. Lippold, J. C. 2015. *Welding Metallurgy and Weldability*. John Wiley and Sons, Hoboken, New Jersey, pp. 85–94.

17. Pumphrey, W. I., and Jennings, P. H. 1948. *Journal of Institute of Metals* (75): 235–256.

18. Borland, J. C. 1960. Generalized theory of super-solidus cracking in welds and castings, *British Welding Journal* (7): 508–512.

19. Matsuda, F., Nakagawa, H., and Sorada, K. 1982. Dynamic observation of solidification and solidification cracking during welding with optical microscope. *Transactions of JWRI* 11: 67–77.

20. Kou, S. 2015. A criterion for cracking during solidification. *Acta Materialia* (88): 366–374.

21. Campbell, J. 2014. Private communications, United Kingdom, June 2.

22. Kou, S. 1996. *Transport Phenomena and Materials Processing*. Hoboken, N.J., John Wiley and Sons, pp. 64–67.

23. Pandat. 2014. Phase diagram calculation software package for Multicomponent Systems, Computherm, LLC, Madison, Wis.

24. PanAluminum. 2014. Thermodynamic database for commercial aluminum alloys, CompuTherm, LLC, Madison, Wis.

25. Cao, G., and Kou, S. 2007. Real-time monitoring of hot tearing in AZ91E magnesium casting. *Transactions of the American Foundry Society* vol. 115, paper 07-034.

26. Cao, G., and Kou, S. 2006. Hot tearing in ternary Mg-Al-Ca alloy castings. *Metallurgical and Materials Transactions* A, vol. 37A, pp. 3647–3663.

27. Cao, G., and Kou, S. 2010. Onset of hot tearing in ternary Mg-Al-Sr alloy castings. *Metallurgical and Materials Transactions* A, vol. 41A, pp. 2139–2150.

28. *Aluminum Standards and Data*. 1982. seventh edition, The Alum Assoc., Washington, D.C., p. 15.

29. *Aluminum Filler Alloy Chart*, AlcoTec Wire Corporation, 2750 Aero Park Drive, Traverse City, Mich., *www.alcotec.com*.

30. *Maxal Guide for Aluminum Welding*. 2012. Maxal International, Inc., *Maxal.com*, (9): 43.

31. Dowd, J. D. 1952. Weld cracking of aluminum alloys. *Welding Journal* (31): 448-s to 456-s.

32. Dudas, J. H., and Collins, F. R. 1966. Preventing weld cracks in high strength aluminum alloys. *Welding Journal* (45): 241-s to 249-s.

33. Singer, A. R. E., and Jennings, P. H. 1947. Hot-shortness of the aluminum-silicon alloys of commercial purity. *Journal of Institute of Metals* (73): 197–212.

34. Rosenberg, R. A., Flemings, M. C., and Taylor, H. F. 1960. Nonferrous binary alloys hot tearing. *Trans. AFS.* 68: 518–528.

35. Cross, C. E., and Olson, D. L. 1986. Hot tearing model to assess aluminum weldability. *Aluminum Alloys Their Physical and Mechanical Properties*, vol. III, conference proceedings, Charlottesville, Va. pp. 1869–1875.

36. Novikov, I. I. 1966. *Hot Shortness of Non-Ferrous Metals and Alloys*, Nauka, Moscow, pp. 220–40.

37. Spittle, J. A., and Cushway, A. A. 1983. Influences of superheat and grain structure on hot-tearing susceptibilities of AI-Cu alloy castings. *Metals Technology* 10.1: 6–13.

38. Pumphrey, W. I., and Lyons, J. V. 1948. Cracking during the casting and welding of the more common binary aluminium alloys. *Journal of Institute of Metals* 74: 439–45.

39. Michaud, E. J., Kerr, H. W., and Weckman, D. C. 1995. Temporal pulse shaping and solidification cracking in laser welded Al-Cu alloys. *Trends in Welding Research,* edited by H. B. Smartt, J. A. Johnson, and S. A. David, ASM International, p. 154.

40. American Society for Metals. 1986. *Binary Alloy Phase Diagrams,* vol. 1 Materials Park, Ohio, ASM International.

41. Nakata, K., and Matsuda, F. 1995. Evaluations of ductility characteristics and cracking susceptibility of aluminum alloys during welding. T*ransactions of JWRI* 24(1): 83–94.

42. Liu, J., and Kou, S. 2015. Effect of diffusion on susceptibility to cracking during solidification. *Acta Materialia* 100: 359–368.

43. Smith, C. S. 1948. Grains, phases, and interfaces — An interpretation of microstructure. *Trans AIME* 175: 15–51.

44. Arata, Y., Matsuda, F., Nakata, K., and Shinozaki, K. 1977. Solidification crack susceptibility of aluminum alloy weld metals (Report II): Effect of straining rate on cracking threshold in weld metal during solidification. *Transactions of JWRI* 6(1): 91–104.

45. Nagaumi, H., Suzuki, S., Okane, T., and Umeda, T. 2006. Effect of iron content on hot tearing of high-strength Al-Mg-Si alloys. *Materials Transactions* 47(11): 2821–2827.

46. Choi, H., Sun, Y., Konishi, H., Kou, S., and Li, X. C. 2013. Nanoparticles-induced superior hot tearing resistance of A206 alloy. *Metallurgical and Materials Transactions* A (44): 1897–1907.